Monthly Notices
of the
ROYAL ASTRONOMICAL SOCIETY

MNRAS **471,** 2321–2333 (2017)
Advance Access publication 2017 June 30

doi:10.1093/mnras/stx1635

A remarkably large depleted core in the Abell 2029 BCG IC 1101

Bililign T. Dullo,[1,2,3]★ Alister W. Graham[4] and Johan H. Knapen[2,3]

[1]*Departamento de Astrofísica y Ciencias de la Atmósfera, Universidad Complutense de Madrid, E-28040 Madrid, Spain*
[2]*Instituto de Astrofísica de Canarias, Vía Láctea S/N, E-38205 La Laguna, Tenerife, Spain*
[3]*Departamento de Astrofísica, Universidad de La Laguna, E-38206 La Laguna, Tenerife, Spain*
[4]*Centre for Astrophysics and Supercomputing, Swinburne University of Technology, Hawthorn, VIC 3122, Australia*

Accepted 2017 June 27. Received 2017 June 27; in original form 2016 November 29

ABSTRACT

We report the discovery of an extremely large ($R_b \sim 2.77$ arcsec ≈ 4.2 kpc) core in the brightest cluster galaxy, IC 1101, of the rich galaxy cluster Abell 2029. Luminous core-Sérsic galaxies contain depleted cores – with sizes (R_b) typically 20–500 pc – that are thought to be formed by coalescing black hole binaries. We fit a (double nucleus) + (spheroid) + (intermediate-scale component) + (stellar halo) model to the *Hubble Space Telescope* surface brightness profile of IC 1101, finding the largest core size measured in any galaxy to date. This core is an order of magnitude larger than those typically measured for core-Sérsic galaxies. We find that the spheroid's V-band absolute magnitude (M_V) of -23.8 mag (∼25 per cent of the total galaxy light, i.e. including the stellar halo) is faint for the large R_b, such that the observed core is 1.02 dex $\approx 3.4\sigma_s$ (rms scatter) larger than that estimated from the R_b–M_V relation. The suspected scouring process has produced a large stellar mass deficit (M_{def}) $\sim 4.9 \times 10^{11}\,M_\odot$, i.e. a luminosity deficit ≈28 per cent of the spheroid's luminosity prior to the depletion. Using IC 1101's black hole mass (M_{BH}) estimated from the M_{BH}–σ, M_{BH}–L and M_{BH}–M_* relations, we measure an excessive and unrealistically high number of 'dry' major mergers for IC 1101 (i.e. $\mathcal{N} \gtrsim 76$) as traced by the large M_{def}/M_{BH} ratios of 38–101. The large core, high mass deficit and oversized M_{def}/M_{BH} ratio of IC 1101 suggest that the depleted core was scoured by overmassive SMBH binaries with a final coalesced mass $M_{BH} \sim (4\text{–}10) \times 10^{10}\,M_\odot$, i.e. $\sim (1.7\text{–}3.2) \times \sigma_s$ larger than the black hole masses estimated using the spheroid's σ, L and M_*. The large core might be partly due to oscillatory core passages by a gravitational radiation-recoiled black hole.

Key words: galaxies: elliptical and lenticular, cD – galaxies: fundamental parameters – galaxies: nuclei – galaxies: photometry – galaxies: structure.

1 INTRODUCTION

Many luminous early-type galaxies brighter than $M_B \sim -20.5 \pm 0.5$ mag contain partially depleted cores. Given the high luminosity of brightest cluster galaxies (BCGs), they are interesting targets for investigating the actions of supermassive black holes (SMBHs), which are themselves capable of creating such cores as a flattening in the inner stellar light distributions (e.g. King & Minkowski 1966; King 1978; Binney & Mamon 1982; Lauer 1985). High-resolution imaging with the *Hubble Space Telescope (HST)* subsequently allowed one to better detect and resolve these cores, including those that are small in angular size and unresolved from the ground (e.g. Crane et al. 1993; Ferrarese et al. 1994; Grillmair et al. 1994; Jaffe et al. 1994; Kormendy et al. 1994; van den Bosch et al. 1994; Forbes, Franx & Illingworth 1995; Lauer et al. 1995; Byun et al. 1996; Gebhardt et al. 1996; Faber et al. 1997; Ravindranath et al. 2001; Rest et al. 2001; Laine et al. 2003; Ferrarese et al. 2006; Kormendy & Bender 2009; Dullo & Graham 2012, 2013, 2014; Rusli et al. 2013; Kormendy & Ho 2013).

Here, we report the discovery of an extremely large ($R_b \sim 2''.77 \pm 0.07 \approx 4.2 \pm 0.1$ kpc) core, in fact, the largest to date, in the Abell 2029 cluster's BCG IC 1101 by fitting the core-Sérsic model to the *HST* light profile of the spheroid. The core-Sérsic model describes the light profile of luminous 'core-Sérsic galaxies' which have an inner light profile with a shallow negative logarithmic slope[1] ($\gamma \lesssim 0.3$) that deviates downward relative to the inward

★ E-mail: bdullo@ucm.es

[1] Lauer et al. (1995, see also Faber et al. 1997; Rest et al. 2001) defined the inner logarithmic slope of the galaxy inner light profiles as $-\gamma$.

extrapolation of the outer Sérsic (1968) $R^{1/n}$ profile (e.g. Graham et al. 2003; Trujillo et al. 2004; Ferrarese et al. 2006; Dullo & Graham 2012, 2013, 2014).

Recent works advocated measuring depleted cores of galaxies using the 'cusp radius ($r_{\gamma=0.5}$)', which was introduced by Carollo et al. (1997) and equals the radius where the negative logarithmic slope of the Nuker model profile equals 0.5 (e.g. Lauer et al. 2007; Postman et al. 2012; López-Cruz et al. 2014). While the cusp radius agrees better with the core-Sérsic radius than the Nuker break radius (Lauer et al. 2007), Dullo & Graham (2012, 2013) warned that the light profile of a coreless galaxy can have a radius where $\gamma = 0.5$.

Cores measured using the core-Sérsic model have typical sizes $R_b \sim$ 20–500 pc (e.g. Trujillo et al. 2004; Ferrarese et al. 2006; Richings, Uttley & Körding 2011; Dullo & Graham 2012, 2013, 2014; Rusli et al. 2013), compared to $R_b \sim 4.2$ kpc for IC 1101. López-Cruz et al. (2014) reported an extremely large ($r_{\gamma=0.5} \approx 4.57$ kpc) core for the Abell 85 cluster's BCG Holm 15A. However, this result has since been questioned (Bonfini, Dullo & Graham 2015; Madrid & Donzelli 2016). Postman et al. (2012) fit the Nuker model (Lauer et al. 1995) to the major-axis light profile of the Abell 2261 BCG and found the hitherto largest core ($r_{\gamma=0.5} \sim 3.2$ kpc), which was recently confirmed by Bonfini & Graham (2016) who fit a 2D core-Sérsic model to the galaxy's image and measured $R_b \sim 3.6$ kpc. The Abell 2261 BCG core is over a factor of 2 larger than the largest core in the Lauer et al. (2007) sample of galaxies ($r_{\gamma=0.5} \sim 1.5$ kpc for NGC 6166, see also Laine et al. 2003).

Theory predicts that central stellar mass deficits are created when a coalescing SMBH binary ejects stars with a collective mass that is on the order of the SMBH mass from the centre of a newly formed 'dry' (gas-poor) galaxy merger remnant via a three-body gravitational scattering process (e.g. Begelman, Blandford & Rees 1980; Ebisuzaki, Makino & Okumura 1991; Milosavljević & Merritt 2001; Merritt 2006). Large depleted cores of galaxies may be generated by ultramassive ($\gtrsim 10^{10}$ $M_\odot$) BH binaries and/or the cumulative actions of SMBH binaries that are created during multiple successive dry mergers (e.g. Milosavljević & Merritt 2001; Merritt 2006). The energy liberated from the orbitally decaying SMBH binary typically ejects stars that are on radial orbits, leaving a relative excess of tangential orbits in the galaxy cores (e.g. Quinlan & Hernquist 1997; Milosavljević & Merritt 2001; Gebhardt et al. 2003; Thomas et al. 2014, 2016). Dullo & Graham (2015) showed that these core regions tend to be round.

Additional core depletion mechanisms can enlarge the stellar mass deficit and the depleted core of galaxies. For example, the SMBH that is produced from the coalesce of the inspiralling SMBH binary may recoil to conserve the linear momentum that is carried away in the other direction by the anisotropic emission of gravitational wave radiation (Bekenstein 1973; Fitchett 1983; Redmount & Rees 1989). Most gravitational wave-recoiled SMBHs have kick velocities lower than their host galaxies' escape velocities (e.g. Gualandris & Merritt 2008). Therefore, the recoiled SMBH ejects yet more stars as it repetitively oscillates in the core region of its host, resulting in a larger depleted core/mass deficit (Boylan-Kolchin, Ma & Quataert 2004; Merritt et al. 2004; Gualandris & Merritt 2008). If the coalesced SMBH does escape the galaxy, then the core expands as it is no longer so tightly bound. Furthermore, Kulkarni & Loeb (2012) proposed that the scouring action of multiple SMBHs generates larger stellar mass deficits than a single SMBH binary due to the SMBH–SMBH encounters. This scenario assumes that multiple SMBHs are present in galaxies at high redshift because of high galaxy merger rates.

Table 1. IC 1101 basic data.

Galaxy	Type	B_T (mag)	σ (km s^{-1})	z
(1)	(2)	(3)	(4)	(5)
IC 1101	BCG	15.3	378	0.0799

Notes. Col. 1: galaxy name. Col. 2: morphological type, the galaxy is classified as an S0 in the RC3 (de Vaucouleurs et al. 1991). Cols. 3–4: total B-band magnitude and central velocity dispersion from HyperLeda (http://leda.univ-lyon1.fr; Paturel et al. 2003). Col. (5): redshift (see Section 1.1).

Using numerical simulations that did not include SMBHs, Goerdt et al. (2010) proposed core generation by a stalled perturber that is captured and dragged to the centre of a galaxy (e.g. Arca-Sedda et al. 2015). In this scenario, the energy transferred from the perturber to the stars at the centre of the galaxy would produce a core (see also Antonini & Merritt 2012; Arca-Sedda, Capuzzo-Dolcetta & Spera 2016).

1.1 IC 1101

IC 1101 is the BCG of the richness class 4.4 galaxy cluster Abell 2029 (Dressler 1978b) at a redshift of $z = 0.0799$ (NED,[2] Virgo + GA + Shapley), see Table 1. A2029 is regarded as one of the most relaxed clusters in the Universe (e.g. Dressler 1979; Buote & Tsai 1996).

Our adopted redshift for IC 1101 gives a luminosity distance of 363 Mpc and a scale of 1.51 kpc arcsec^{-1}.

Section 2 describes the data reduction, the surface brightness profile and isophotal parameter extraction techniques. In Section 3, we discuss the analytic model fit to the light profiles of IC 1101 together with the analysis of our four-component decompositions. In Sections 3.3 and 3.4, we discuss the colour map and the isophotal properties, respectively, of IC 1101 in the context of our light profile decompositions. Section 4.1 discusses past works on IC 1101 and similar BCGs. Section 4.2 compares the large depleted core of IC 1101 with those of other core galaxies in the literature. In Section 4.3, we discuss the stellar mass deficit of IC 1101. Section 4.4 discusses a possible formation scenario for IC 1101 and Section 5 summarizes our main conclusions.

2 DATA

2.1 *HST* imaging

High-resolution *HST* Wide-Field Planetary Camera 2 (WFPC2) and Planetary Camera 1 (PC1) images of IC 1101 taken with *F*450*W* and *F*702*W* filters were retrieved from the public Hubble Legacy Archive (HLA).[3] These images were obtained under a proposal ID 6228 (PI: Trauger). Fig. 1 reveals the remarkably flattened core of IC 1101 imaged with PC1 chip of the WFPC2 camera.

While the *HST* WFPC2 images obtained from the HLA archive have a 160 arcsec × 160 arcsec L-shaped field of view (FOV) at an image scale of 0.1 arcsec pixel^{-1}, the PC1 images with a plate scale of 0.05 arcsec pixel^{-1} have a 40 arcsec × 40 arcsec FOV (Fig. 2).

[2] We assume a cosmology with $H_0 = 70$ km s^{-1} Mpc^{-1}, $\Omega_\Lambda = 0.7$ and $\Omega_m = 0.3$.
[3] http://hla.stsci.edu

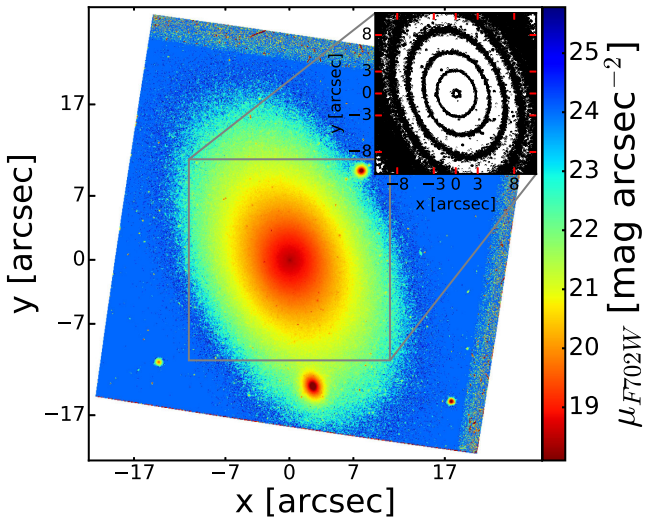

Figure 1. *HST* PC1 *F702W* image of the A2029-BCG IC 1101, showing the large depleted core with break radius surface brightness of $\mu_{b,\,F702W} \sim 19.4$ mag arcsec^{-2}. The top inset shows the contour levels 18.6, 19.3, 20.1, 20.8, 21.6, 22.5, 23.3 × mag arcsec^{-2}). North is up and east is to the left.

2.2 Surface brightness profiles

Our 1D data reduction steps, along with the surface brightness profile extraction procedures follow those in Dullo & Graham (2014, their section 2.3). We used the IRAF[4] ELLIPSE task (Jedrzejewski 1987) to extract surface brightness, ellipticity ($\epsilon = 1 - b/a$), position angle (PA), and isophote shape parameter (B_4) profiles from the high-resolution *HST* WFPC2 *F450W* and *F702W* images of IC 1101 (see Fig. 2). A mask was created first by running SEXTRACTOR (Bertin & Arnouts 1996) on the galaxy image and then combining this with a careful manual mask to exclude all objects except the BCG, and to avoid the gaps between individual CCD detectors and the partially missing quadrant of the WFPC2 images (Fig. 2). We ran ELLIPSE by holding the isophote centres fixed but allowing ϵ and PA to vary. Fig. 2 (middle) shows the resulting isophotes. Fig. 3 (left) shows a residual image that is produced by subtracting the model image of the ellipse fit from the science image.

2.2.1 *Sky background*

We focus on the *HST* WFPC2 *F702W*-band light profile of IC 1101 in this work instead of the *F450W*-band light profile to minimize the effects of young stellar populations and dust contamination, although this galaxy appears to be dust free. Fig. 2 shows that the outermost corner of the WF3 chip of the WFPC2 is mostly free from IC 1101's light, suggesting optimum sky-background level determination by the HLA pipeline. However, because IC 1101 extends beyond the WFPC2 CCDs (Fig. 2), poor sky-background subtraction can bias the extracted profile at low surface brightness. Concerned about this, we extracted light profiles from the mosaic SDSS *r*- and *z*-band images of IC 1101 (Fig. 4), with a 5 arcmin × 5 arcmin FOV, using ELLIPSE. We found that the *HST F702W* and SDSS *z*-band profiles agree very well but they differ slightly from the SDSS *r*-band profile at large radii (Fig. 5). This discrepancy is due to a poor background subtraction of the SDSS *r*-band image by the SDSS pipeline, resulting in a non-uniform background that can be seen in the image as dark and bright stripes (see Blanton et al. 2011). None the less, in Section 3, we model a composite (*HST F702W* plus SDSS *r* band) profile of the galaxy and find that the discrepancy between the *HST* and SDSS *r*-band profiles did not affect the conclusions in the paper.

We quote all magnitudes in the VEGA magnitude system.

3 DECOMPOSING IC 1101

3.1 1D decomposition

We fit a (core-Sérsic spheroid) plus (Sérsic intermediate-scale component) plus (exponential halo) plus (smaller inner Gaussian component) to the *HST F702W* and *F450W* brightness profiles of IC 1101 (Figs 6 and 7).

The Sérsic (1963) model describes the surface brightness profiles of low- and intermediate-luminosity ($M_B \gtrsim -20.5$ mag) spheroids (see the review by Graham & Driver 2005, and references therein). This model is defined as

$$I(R) = I_{\rm e} \exp\left[-b_n \left(\frac{R}{R_{\rm e}}\right)^{1/n} - 1\right], \quad (1)$$

where $I_{\rm e}$ denotes the intensity at the half-light radius ($R_{\rm e}$). The quantity $b_n \approx 2n - 1/3$, for $1 \lesssim n \lesssim 10$ is defined as a function of the Sérsic index n such that $R_{\rm e}$ encloses half of the total luminosity. For $n = 0.5$ and 1, the Sérsic model is a Gaussian function and an exponential function, respectively.

As noted in the Introduction, luminous ($M_B \lesssim -20.5$ mag) galaxies possess central stellar deficits such that their inner light profiles depart downwards relative to the inward extrapolation of the outer Sérsic profile. The core-Sérsic model,[5] a combination of an inner power-law core and an outer Sérsic profile with a transition region, describes very well the underlying light profiles of spheroids with depleted cores. The core-Sérsic model is written as

$$I(R) = I' \left[1 + \left(\frac{R_{\rm b}}{R}\right)^{\alpha}\right]^{\gamma/\alpha} \exp\left[-b\left(\frac{R^{\alpha} + R_{\rm b}^{\alpha}}{R_{\rm e}^{\alpha}}\right)^{1/(\alpha n)}\right], \quad (2)$$

with

$$I' = I_{\rm b} 2^{-\gamma/\alpha} \exp\left[b(2^{1/\alpha} R_{\rm b}/R_{\rm e})^{1/n}\right], \quad (3)$$

where $I_{\rm b}$ is intensity at the core break radius $R_{\rm b}$, γ is the slope of the inner power-law region and α moderates the sharpness of the transition between the inner power-law core and the outer Sérsic profile. $R_{\rm e}$ and b are defined as in the Sérsic model.

Figs 6 and 7 show a four-component decomposition of the *HST F702W* geometric mean radius ($\sqrt{ab}$) and semimajor axis light profiles of IC 1101 into a spheroid, an intermediate-scale component, an outer stellar halo and small Gaussian for the extended nucleus apparent in the ellipticity profile. The fit residuals and the root-mean-square (rms) residuals are also shown. The best-fitting parameters that match the data are calculated by iteratively minimizing the rms residuals using the Levenberg–Marquardt optimization algorithm (see Dullo & Graham 2014; Dullo, Martínez-Lombilla

[4] IRAF is distributed by the National Optical Astronomy Observatory, which is operated by the Association of Universities for Research in Astronomy (AURA) under cooperative agreement with the National Science Foundation.

[5] Because the core-Sérsic model gives a good description of galaxies with depleted cores, we refer to such galaxies as 'core-Sérsic galaxies'.

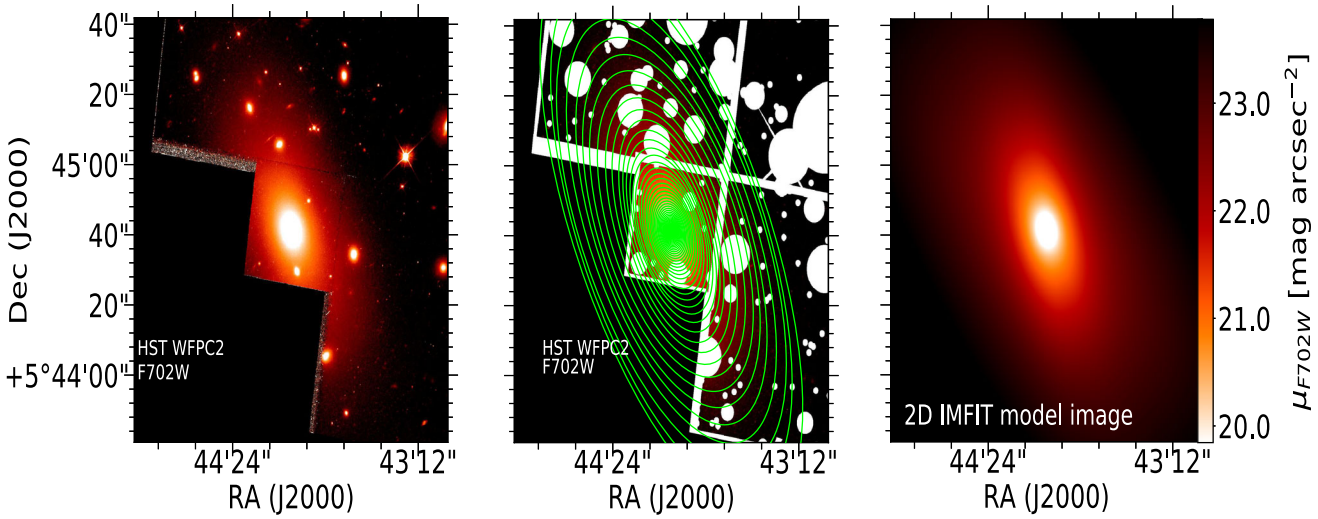

Figure 2. Left-hand panel: *HST* WFPC2 *F*702*W* image of IC 1001. Middle panel: masked regions (i.e. white areas) and isophotes from IRAF ELLIPSE overplotted on the *HST* image. Right-hand panel: IMFIT model image of IC 1101 (see Section 3).

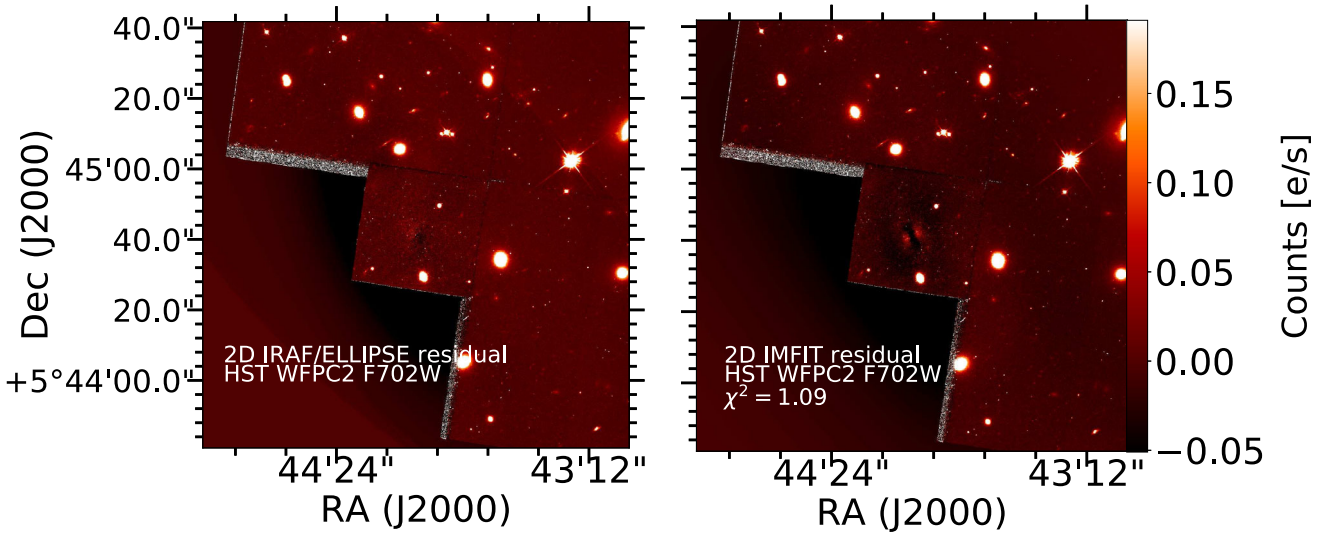

Figure 3. Left-hand panel: residual image that is created after subtracting a model image (generated by the IRAF BMODEL task) from the original *HST* WFPC2 *F*702*W* image shows positive and negative residuals to the NE and SW of the core, respectively. This suggests that the core is somewhat offset with respect to the outer isophotes, consistent with the scenario where the depleted core is enlarged through oscillatory core passages by a gravitational radiation-recoiled black hole (see Postman et al. 2012 and Section 4). The top right and bottom left regions of this residual image are outside the IRAF BMODEL image of IC 1101 (see Fig. 2, middle panel). Right-hand panel: IMFIT residual image. The residual structure inside $R \sim 10$ arcsec is due to IC 1101's ellipticity gradient which is not well represented by the IMFIT core-Sérsic model component with $\epsilon \sim 0.24$ that dominates at $R \lesssim 10$ arcsec (see the text for details). The count rates in the residual images that are shown in units of electrons per second and the 2D surface brightness μ_{F702W} (mag arcsec^{-2}, Fig. 2) are related as $\mu_{F702W} = -2.5$ log (count rates) + 19.547.

& Knapen 2016). For each iteration, the profiles of individual model components were convolved with the Gaussian point spread function (PSF) and then summed to create the final model profile. The ellipticity was taken into account when convolving the major-axis light profiles (see Trujillo et al. 2001a,b). The full widths at half-maximum (FWHMs) of the PSFs were measured using several stars in the galaxy image. While we focus throughout this paper on the 1D fit to the *HST F*702*W* light profiles convolved with the Gaussian PSF, we also performed a 1D fit to IC 1101's *HST F*450*W* light profile and to the *HST F*702*W* light profile convolved with the Moffat PSF to check the discrepancies in fit parameters arising from using the *F*702*W*- and *F*450*W*-band images, and our treatment of the PSF (Fig. 7). We found good agreement between the fits to the *F*702*W*- and *F*450*W*-band profiles. Also, Figs 6 and 7 reveal an excellent agreement between the fits convolved with the Gaussian and Moffat PSFs. We note that the *HST* WFPC2 PSF is better described by the Moffat function than the Gaussian function. However, our Gaussian and Moffat PSF-convolved fits agree very well because IC 1101 has a flat core. Tables 2 and 3 list the best-fitting model parameters from the 1D decompositions.

The four-component (core-Sérsic spheroid) plus (Sérsic intermediate-scale component) plus (exponential halo) plus (Gaussian nuclear component) model yields an excellent fit to both the geometric mean profile and the major-axis profile of IC 1101, revealed by very small rms residuals of 0.016 and 0.013 mag arcsec^{-2}, respectively (Fig. 6). The initial fit to the light profile of IC 1101

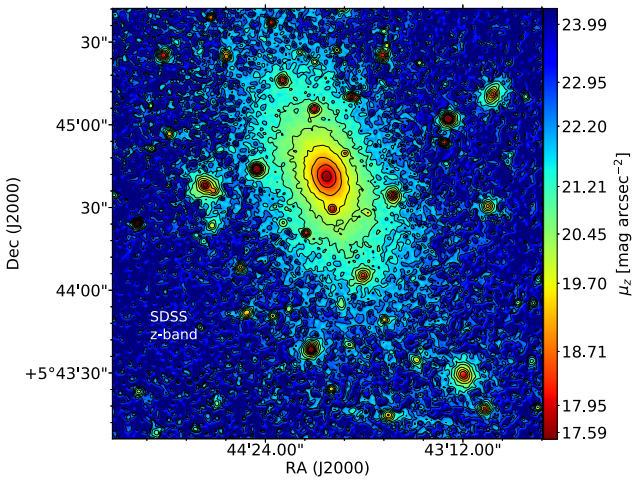

Figure 4. SDSS z-band image and contour plot of IC 1101 smoothed with a Gaussian (FWHM ∼1.5 arcsec), highlighting the intermediate-scale and stellar halo components.

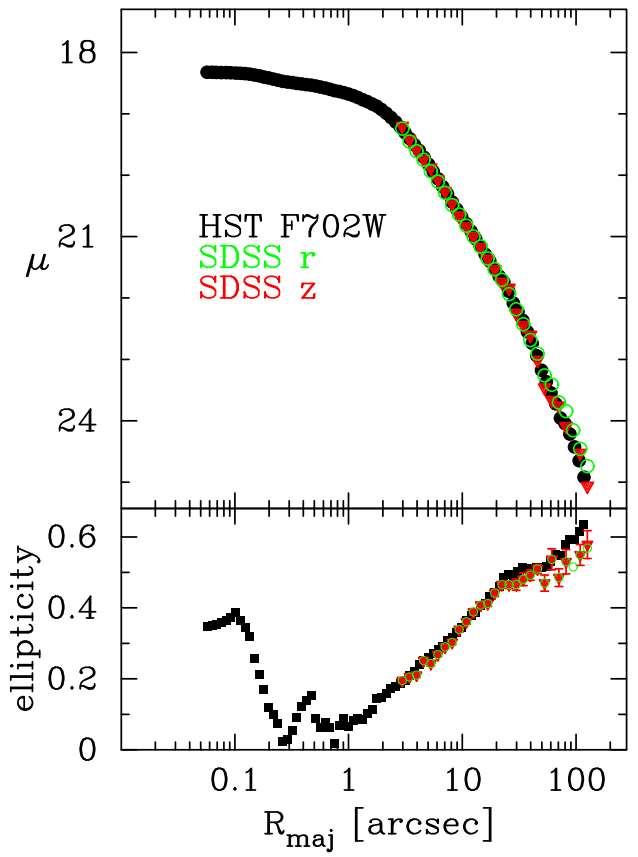

Figure 5. Major-axis *HST F702W*- and SDSS z- and r-band surface brightness and ellipticity profiles of IC 1101 denoted by black dots, red triangles and open green circles, respectively. The SDSS r- and z-band data are zero-pointed to the *HST F702W* profile. For clarity, we only show the error bars on the SDSS z-band ellipticities.

using a core-Sérsic model was inadequate, as the intermediate-scale and halo components caused obvious residual structures. Adding a halo component improved our fit, but from the fit and the residual profile it was clear that an additional intermediate-scale component and a small central Gaussian component are also present in the galaxy. Our adopted four-component decomposition (Fig. 6, left and middle panels) is supported by the galaxy colour, velocity dispersion profile and isophotal properties (see Sections 3.3 and 3.4). The fit to the geometric mean radius gives a core-Sérsic spheroid with a break radius of $R_b \sim 2\farcs52 \pm 0.07 \approx 3.8 \pm 0.1$ kpc and a Sérsic index of $n \sim 6.3$, while the major-axis fit yielded $R_b \sim 2\farcs77 \pm 0.07 \approx 4.2 \pm 0.1$ kpc and $n \sim 5.6$. IC 1101 has the largest core size ($R_{b,\,maj} \sim 4.2$ kpc) to date. The 'intermediate-scale component' has a low ($n \sim 0.62$) Sérsic stellar light distribution (Table 2). The outer halo light of IC 1101 is well fit by an exponential ($n = 1$) function (e.g. Seigar, Graham & Jerjen 2007; Pierini et al. 2008), and the inner Gaussian component has an apparent *F702W* magnitude of 22.8 mag.

Inside $R \sim 0.2$ arcsec, the ellipticity of IC 1101 increases from $\epsilon \sim 0.1$ to $\epsilon \sim 0.4$ towards the centre, which seems to suggest the presence of a nuclear disc (Fig. 6). Also, the isophotes of the galaxy are discy (i.e. $B_4 > 0$) inside $R \sim 0.1$ arcsec. PSF tends to circularize the isophotes. Using *HST* WFPC2 images, Rest et al. (2001) noted that the subpixel interpolation routine of the IRAF task can underestimate the isophote ellipticity and generate artificial deviations from pure ellipses at $R \lesssim 0.2$ arcsec (see also Jedrzejewski 1987). However, as noted above IC 1101 has isophotes with high ellipticities at $R \lesssim 0.2$ arcsec. The faint nuclear component of IC 1101 may be due to an unresolved double nucleus which is produced by a low-luminosity active galactic nucleus (AGN) and the left-over stellar nuclei of an accreted satellite that was tidally disrupted by the central SMBH. The elliptical galaxies NGC 4486B, VCC 128 and NGC 5419 contain two central point sources separated by 12, 32 and 70 pc, respectively, that created a double nucleus with high ellipticity and positive B_4 values (see Lauer et al. 1996, their figs 3 and 4; Lauer et al. 2005; Debattista et al. 2006; Dullo & Graham 2012; Mazzalay et al. 2016). The NRAO VLA Sky Survey (NVSS; Condon et al. 1998), with a resolution of 45 arcsec, has detected a radio source at 1.4 GHz with an integrated flux of 527 ± 18.2 mJy. This source has an optimal location 4 arcsec south-west of IC 1101's centre, favouring the presence of an AGN in IC 1101. NVSS has also detected a weaker radio source with an integrated flux of 5.3 ± 0.5 mJy located ∼50 arcsec away from the stronger source. We cannot rule out the possibility of a dual AGN near/at the centre of IC 1101.

As discussed in Section 2.2.1, the *HST F702W* and SDSS r-band light profiles somewhat disagree at large radii ($R \gtrsim 40$ arcsec) due to a poor sky-background subtraction by the SDSS pipeline (Fig. 5). We checked on the level of this discrepancy between the profiles by fitting a four-component (core-Sérsic spheroid) plus (Sérsic intermediate-scale component) plus (exponential halo) plus (inner Gaussian) model to a composite light profile, i.e. *HST F702W* profile at $R \lesssim 40$ arcsec plus SDSS r-band data over $R > 40$ arcsec (Fig. 6). This fit agrees with the one done using the *HST F702W* light profile (see Fig. 6 and Tables 2 and 3) and therefore suggests that the sky-background subtraction is not a big issue.

A key point highlighted by Dullo & Graham (2012, 2013) is the misclassification of (low-luminosity $M_B \gtrsim -20.5$ mag) coreless galaxies with low Sérsic index profiles as galaxies with depleted cores by the Nuker model. A PSF-convolved four-component Sérsic spheroid + Sérsic intermediate-scale component + exponential halo + (inner) Gaussian fit fails to describe the geometric-mean light profile of IC 1101 (Fig. 7). This fit yields a near exponential ($n = 1.04$) profile to approximate the core-Sérsic spheroid profile, and an intermediate Sérsic model component with a half-light radius surface brightness $\mu_e \sim 22.3$, ∼0.5 mag arcsec^{-2} brighter than that of our adopted geometric-mean fit, $\mu_e \sim 22.8$ mag

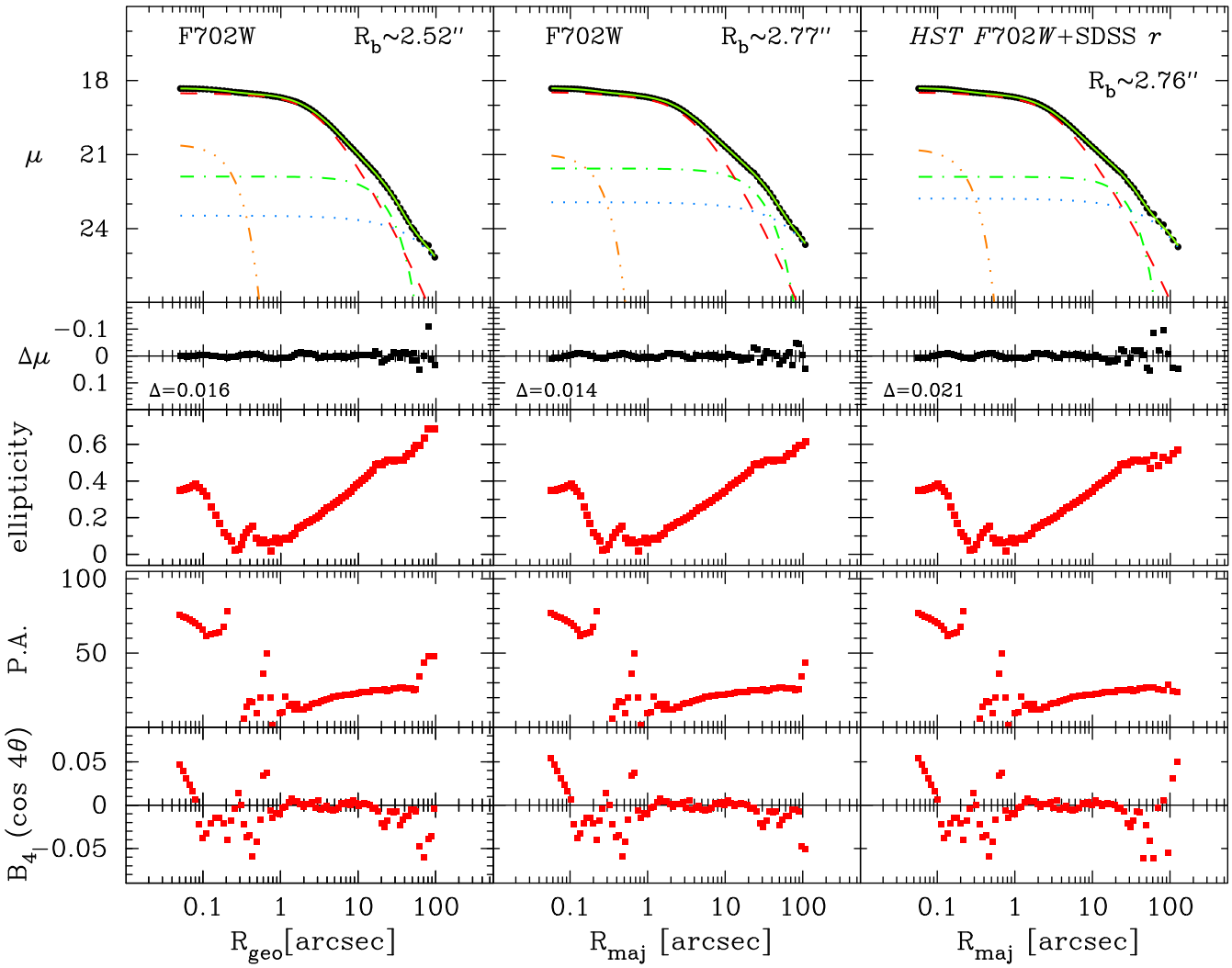

Figure 6. 1D multicomponent decompositions of the (i) *HST F702W*-band geometric mean ($\sqrt{ab} = a\sqrt{(1-\epsilon)}$) surface brightness profile (left), (ii) *HST F702W*-band semimajor axis profile (middle) and (iii) composite semimajor axis profile (i.e. *HST F702W*-band profile at $R \lesssim 40$ arcsec plus SDSS *r*-band profile at $R > 40$ arcsec) of IC 1101. From top to bottom, the panels show Gaussian nuclear component (triple dot–dashed curve) + core-Sérsic spheroid (dashed curve) + Sérsic intermediate-component (dot–dashed curve) + exponential halo (dotted curve) model fits together with the rms residuals about the fits, ellipticity (ϵ), position angle (PA, measured in degrees from north to east) and isophote shape parameter (B_4) profiles for the galaxies. The models have been convolved with the PSF (see the text for details).

arcsec^{-2} (Table 2). The pattern in the residual profile between 0.2 arcsec $\lesssim R \lesssim$ 3 arcsec reveals the presence of a depleted core in the galaxy (Fig. 7).

3.2 2D decomposition

We fit a 2D model, comprising a Gaussian nuclear component, a core-Sérsic spheroid, a Sérsic intermediate-scale component and an exponential stellar halo, to the WFPC2 *F702W* image of IC 1101 using IMFIT[6] (Erwin 2015) and the mask image from the IRAF ELLIPSE run (Section 2.2). Fig. 2 (right) shows this model image that was convolved with a TINYTIM WFPC2 PSF (Krist 1995). Fig. 3 (right) shows the pertaining IMFIT residual image created after subtracting the model image from the galaxy image. In general, the agreement between the 1D and 2D decompositions is good, but the $\mu_{0,\mathrm{h}}$ of the 2D halo is brighter than that of the 1D one (see Figs 2 and 3, and Tables 2, 3 and 4). However, because each IMFIT galaxy component is associated with a single ellipticity, PA and isophote shape parameter, IC 1101's ellipticity gradient over $R \lesssim 4$ arcsec was not well represented by our best $\epsilon \sim 0.24$ core-Sérsic model component that dominates other fit components at $R \lesssim 10$ arcsec, resulting in the residual structure (see Figs 2, 3 and 6). Bonfini et al. (2015, their fig. 4) also performed 2D core-Sérsic+exponential and Sérsic+exponential fits to the 2D light distribution of the BCG Holm 15A with outwardly rising ellipticity using the GALFIT-CORSAIR software (Bonfini 2014) and found residual structures similar to that shown in Fig. 3 (right). Ciambur (2016) presents a discussion regarding the pros and cons of how galaxy images are modelled, including a discussion of the benefits of modelling 1D light profiles. We prefer our 1D decompositions and focus on them throughout the paper, but the good agreement between the 1D and 2D fit parameters, except for $\mu_{0,\mathrm{h}}$, implies that the main conclusions in this paper remain unchanged if we choose our 2D decomposition.

[6] http://www.mpe.mpg.de/erwin/code/imfit/

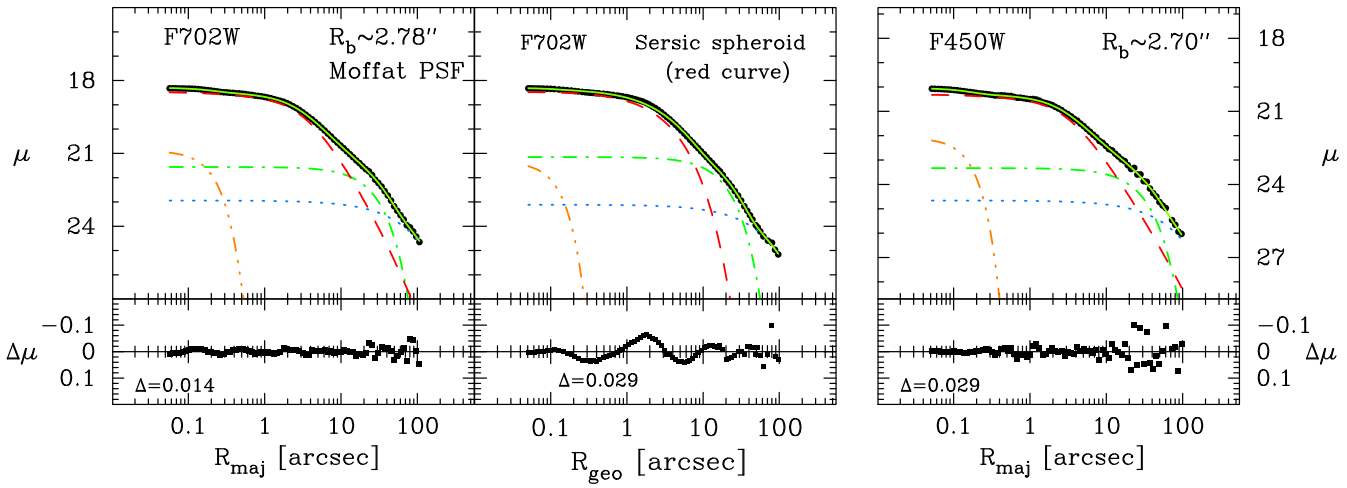

Figure 7. Left-hand panel: similar to Fig. 6 (middle) but showing here a four-component fit convolved with a Moffat PSF. Middle panel: a Gaussian nuclear component (triple dot–dashed curve) + Sérsic spheroid (dashed curve) + Sérsic intermediate-component (dot–dashed curve) + exponential halo (dotted curve) fit to the *F*702*W*-band geometric mean surface brightness profile of IC 1101. Our fitting code attempts to fit a near exponential ($n \sim 1$) Sérsic model to what is actually a core-Sérsic light distribution of the Spheroid with $n \sim 6.3$, yielding a snake-like residual structure at $R \gtrsim 0.2$ arcsec and a brighter intermediate-scale component than that of our adopted fit (see Section 3). Right-hand panel: similar to Fig. 6 (middle) but showing here a four-component fit to the WFPC2 *F*450*W* light profile.

Table 2. Structural parameters.

Galaxy	μ_b	R_b (arcsec)	R_b (kpc)	γ	α	n_{cS}	$R_{e,cS}$ (arcsec)	$R_{e,cS}$ (kpc)	$\mu_{e,S}$	n_S	$R_{e,S}$ (arcsec)	$R_{e,S}$ (kpc)	$\mu_{0,h}$	h (arcsec)	h (kpc)	m_{pt} (mag)
(1)	(2)	(3)	(4)	(5)	(6)	(7)	(8)	(9)	(10)	(11)	(12)	(13)	(14)	(15)	(16)	(17)
1D fit/HST *F702W*																
IC 1101	19.33	2.52	3.8	0.05	2	6.32	5.3	8.0	22.81	0.62	19.5	29.4	23.41	58.6	88.5	22.8

Notes. Structural parameters from the 1D Gaussian nuclear component + core-Sérsic spheroid + Sérsic intermediate-component + exponential halo model fit to the *HST F*702*W* geometric-mean-axis surface brightness profiles of IC 1101 (Fig. 6). The fit was convolved with a Gaussian PSF. Col. 1: galaxy name. Cols 2–9: best-fitting parameters from the core-Sérsic model. Cols 10–13: Sérsic model parameters for the intermediate-scale component. Cols 14–16 best-fitting parameters for the exponential halo light. Col. 17: apparent *F*702*W* magnitude of the unresolved double nucleus. μ_b, μ_e and $\mu_{0,h}$ are in mag arcsec^{-2}. The core-Sérsic spheroid has a total *F*702*W*-band absolute magnitude $M_{Sph} \sim -24.3$ mag. The intermediate component has a total *F*702*W*-band absolute magnitude $M_{Int} \sim -23.9$ mag. These magnitudes are *not* corrected for Galactic dust extinction, $(1+z)^4$ surface brightness dimming and stellar evolution from $z \sim 0.08$ to the present day. We estimate that the uncertainties on the core-Sérsic parameters R_b, γ, n_{cS} and $R_{e,cS}$ are ~ 2.5 per cent, 10 per cent, 20 per cent and 25 per cent, while the uncertainties associated with the Sérsic parameters n_S, $R_{e,S}$ and the exponential scalelength h are ~ 20 per cent, 25 per cent and 10 per cent, respectively. The uncertainties on μ_b, $\mu_{e,S}$ and $\mu_{0,h}$ are ~ 0.02, 0.2 and 0.2 mag arcsec^{-2}, respectively. These errors on the fit parameters were estimated following the techniques in Dullo & Graham (2012, their section 4).

Table 3. Structural parameters.

Galaxy	μ_b	R_b (arcsec)	R_b (kpc)	γ	α	n_{cS}	$R_{e,cS}$ (arcsec)	$R_{e,cS}$ (kpc)	$\mu_{e,S}$	n_S	$R_{e,S}$ (arcsec)	$R_{e,S}$ (kpc)	$\mu_{0,h}$	h (arcsec)	h (kpc)	m_{pt} (mag)
(1)	(2)	(3)	(4)	(5)	(6)	(7)	(8)	(9)	(10)	(11)	(12)	(13)	(14)	(15)	(16)	(17)
1D fit/HST *F702W*																
IC 1101	19.35	2.77	4.2	0.08	2	5.60	7.7	11.6	22.68	0.67	26.2	39.5	22.94	66.70	100.7	23.1
1D fit/HST *F702W* + *SDSS* r																
IC 1101	19.33	2.76	4.2	0.08	2	6.29	9.8	14.8	22.74	0.58	24.1	36.4	22.80	69.24	104.6	23.1
1D fit/HST *F702W (Moffat PSF)*																
IC 1101	19.33	2.78	4.2	0.08	2	5.70	7.7	11.6	22.67	0.65	26.2	39.5	22.94	67.12	101.4	23.0
1D fit/HST *F450W*																
IC 1101	21.14	2.65	4.0	0.07	2	7.50	13.1	19.8	24.52	0.71	30.0	45.3	24.66	66.83	100.9	24.8

Notes. Same as Table 2 but here showing semimajor axis structural parameters from the fits to the *HSTF*702*W*, *HSTF*450*W* and composite (*HST F702W* plus SDSS *r* band) profiles of IC 1101. We also provide fit parameters from the 1D fit to the *HSTF*702*W* light profile of the galaxy convolved with a Moffat PSF.

3.3 Colour map

Fig. 8 shows the WFPC2 *F*450*W* − *F*702*W* colour map for IC 1101, indicating that there is no obvious localized dust absorption. To create this colour map, the WFPC2/*F*450*W* and WFPC2/*F*702*W* images were aligned to better than 0.2 arcsec using stars in the images with the IRAF GEOMAP and GEOTRAN tasks. We did not worry about the difference between the PSFs of the WFPC2/*F*450*W* and WFPC2/*F*702*W* images. The galaxy becomes gradually bluer

Table 4. Structural parameters.

Galaxy	μ_b	R_b	R_b	γ	α	n_{cS}	$R_{e,cS}$	$R_{e,cS}$	P.A.$_{cS}$	ϵ_{cS}	$\mu_{e,S}$	n_S	$R_{e,S}$	$R_{e,S}$	PA$_S$	ϵ_S	$\mu_{0,h}$	h	h	PA$_h$	ϵ_h	m_{pt}
		(arcsec)	(kpc)				(arcsec)	(kpc)	(°)				(arcsec)	(kpc)	(°)			(arcsec)	(kpc)	(°)		(mag)
(1)	(2)	(3)	(4)	(5)	(6)	(7)	(8)	(9)	(10)	(11)	(12)	(13)	(14)	(15)	(16)	(17)						
2D fit/HST *F702W*																						
IC 1101	19.39	2.79	4.4	0.14	2.4	6.4	5.4	8.2	18.4	0.24	22.29	0.65	19.1	28.8	21.1	0.57	22.24	57.7	87.1	38	0.50	22.91

Notes. Similar to Table 2 but here showing structural parameters from the 2D IMFIT (nuclear component + core-Sérsic spheroid + Sérsic intermediate-component + exponential halo) model image fit to the *HST*/*F702W*-band image. The IMFIT isophote shape parameter $c_{0,S}$, not to be confused with that of the IRAF/ELLIPSE B_4, is positive/negative for boxy/discy isophotes (Erwin 2015). We found $c_{0,S} \sim 0.61 \pm 0.007$ and $c_{0,h} \sim 0.79 \pm 0.007$ for the intermediate-component and outer halo. The uncertainties from IMFIT associated with R_b, γ, α, n_{cS}, $R_{e,cS}$, P.A.$_{cS}$, ϵ_{cS}, n_S, $R_{e,S}$, PA$_S$, ϵ_S, h, PA$_h$, ϵ_h are ~ 0.6 per cent, 0.3 per cent, 0.3 per cent, 0.4 per cent, 0.8 per cent, 0.3 per cent, 0.3 per cent, 0.9 per cent, 0.3 per cent, 0.3 per cent, 0.4 per cent, 0.3 per cent and 0.3 per cent. The uncertainties on μ_b, $\mu_{e,S}$ and $\mu_{0,h}$ are ~ 0.01 mag arcsec^{-2}, 0.01 mag arcsec^{-2} and 0.02 mag arcsec^{-2}, respectively.

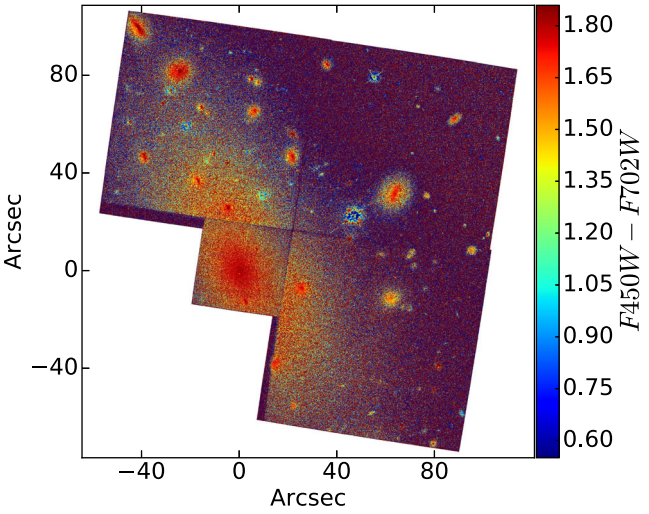

Figure 8. *HST* WFPC2 $F450W - F702W$ colour map of IC 1101 shows that the galaxy becomes bluer with increasing radius, in good agreement with our brightness profile decomposition (Fig. 6). The regions where the intermediate component and the halo light dominate are bluer than that dominated by the spheroid.

at larger radii where the intermediate-scale component and the halo light dominate compared to the inner region with a high concentration of old stars from the spheroid. As noted in Section 3.1, we found good agreement between the 1D $F450W$-band and $F702W$-band light profile decompositions (Figs 6 and 7). The slight discrepancies in the fit parameters are attributed to the galaxy colour gradient.

3.4 Ellipticity, position angle and isophote disciness/boxiness

Excluding the most PSF-affected region (i.e. $R \lesssim 0.2$ arcsec, see Section 3), IC 1101 has an ellipticity of 0.1 ± 0.08 within the break radius $R_b = 2.52$ arcsec, in good agreement with the observations by Dullo & Graham (2015) who showed that core-Sérsic galaxies tend to have round cores, i.e. $\epsilon\ (R = R_b) \lesssim 0.2$. The ellipticity of IC 1101 increases steadily from ~ 0.2 to 0.5 with increasing radius over 3 arcsec $\lesssim R_{geo} \lesssim 20$ arcsec, it remains roughly constant (i.e. $\epsilon \sim 0.5$) at radii dominated by the intermediate-scale component (20 arcsec $\lesssim R_{geo} \lesssim 40$ arcsec) and then increases again at large radii ($R_{geo} \gtrsim 40$ arcsec) where the halo light dominates (Figs 4, 5 and 6). The trend of increasing ellipticity with radius has been observed for other BCGs (e.g. Porter, Schneider & Hoessel 1991; Postman & Lauer 1995; Gonzalez, Zabludoff & Zaritsky 2005, their fig. 10; Khosroshahi, Ponman & Jones 2006; Bender et al. 2015, their fig. 7).

The major axis of IC 1101 is oriented in the south-west to north-east direction (Figs 2, 4 and 6). The spheroid and the intermediate-scale component are very well aligned with only a modest twist of $\sim 5^\circ$. The outer halo is twisted by $\sim 20^\circ$ from the intermediate-scale component. The shape and orientation of the halo of IC 1101 are comparable to those of the surrounding cluster galaxies, suggesting a strong connection between the cluster galaxies and the host cluster's gravitational potential (Dressler 1978a,b, 1979).

The isophotes of IC 1101 are predominantly boxy (i.e. $B_4 < 0$) at 0.1 arcsec $\lesssim R_{geo} \lesssim 1$ arcsec and $R_{geo} \gtrsim 20$ arcsec (Figs 1, 4 and 6). The galaxy has pure elliptical (i.e. $B_4 = 0$) isophotes over 1 arcsec $\lesssim R_{geo} \lesssim 20$ arcsec.

4 DISCUSSION

4.1 Past work on IC 1101 and similar BCGs

BCGs have been shown to contain excess halo light at large radii with respect to the de Vaucouleurs (1948) $R^{1/4}$ model fit to the main body of the BCG that is embedded within the halo light (e.g. Oemler 1976; Carter 1977; Dressler 1981; Lugger 1984; Schombert 1986). However, a single-component $R^{1/n}$ galaxy will 'appear' to have a halo if $n > 4$.[7] Gonzalez et al. (2005) and Zibetti et al. (2005) fit an $R^{1/4}$ spheroid plus an $R^{1/4}$ outer halo light model to the light profiles of their BCGs before Seigar et al. (2007) showed that most BCGs in their sample are well described by a Sérsic ($R^{1/n}$) spheroid plus an exponential ($n = 1$) halo model, excluding the core regions (see also Pierini et al. 2008). Donzelli, Muriel & Madrid (2011) also found that roughly half of their 430 BCGs are well fit by a Sérsic spheroid plus an outer exponential model.

IC 1101 and its host cluster (A2029) have been extensively studied (e.g. Matthews, Morgan & Schmidt 1964; Dressler 1978a,b, 1979; Stewart et al. 1984; Schombert 1987; Porter et al. 1991; Uson, Boughn & Kuhn 1991; Sembach & Tonry 1996; Carter, Bridges & Hau 1999; Kelson et al. 2002). As noted in Section 3, IC 1101 has an intermediate-scale component plus an exponential stellar halo that dominate over the spheroid's core-Sérsic stellar light distribution at large radii. Computing the total integrated flux for each model component (Fig. 6) using the best-fitting structural parameters (Table 2) yields total light fractions for the spheroid, intermediate-scale component and outer halo component equal to 25.1 per cent, 17.4 per cent and 57.5 per cent, respectively. The total flux fraction of the unresolved double nucleus is negligible.

The intermediate-scale component plus the outer stellar halo and the outwardly rising ellipticity profile (Fig. 6 and Section 3.4) are the likely reasons why IC 1101 is classified as a lenticular galaxy in the RC3 (de Vaucouleurs et al. 1991). IC 1101 shows almost no rotation ($V_{\rm rot} \sim 0\,{\rm km\,s^{-1}}$) within 13 kpc (Dressler 1979, his fig. 4b; Fisher, Illingworth & Franx 1995, their fig. 5b). At $R \gtrsim 13$ kpc, Dressler (1979, his fig. 4b) measured $V_{\rm rot} \sim$50–150 km s^{-1} but he warned that those results were tentative. Importantly, Dressler (1979, his Fig. 5) showed that the velocity dispersion (σ) of IC 1101 increases outward from 375 km s^{-1} within $R \sim 5$ kpc to $\sim 425 \pm 25\,{\rm km\,s^{-1}}$ for 6 kpc $\lesssim R \lesssim$ 62 kpc before rising to $\gtrsim$500 km s^{-1} beyond $R \sim 62$ kpc (see also Carter et al. 1985; Sembach & Tonry 1996, their fig. 6). Not only is this $\sigma(R)$ profile consistent with our multicomponent light profile decomposition, the low $V_{\rm rot}/\sigma$ ratio also indicates the absence of a disc confirmed by the boxy isophotes ($B_4 < 0$) at $R \gtrsim 20$ arcsec. Akin to IC 1101, NGC 6166 (A2199-BCG) that possesses the largest core ($r_{\gamma'=0.5} \sim 1.5$ kpc) in the Lauer et al. (2007) sample of 219 galaxies also has outwardly rising velocity dispersion and ellipticity profiles (e.g. Fisher et al. 1995; Carter et al. 1999; Kelson et al. 2002; Bender et al. 2015). The reason for a radially increasing velocity dispersion profile is the greater contribution from halo stars, which traces the cluster potential rather than the BCG potential.

While the de Vaucouleurs $R^{1/4}$ model fit by Schombert (1987, his fig. 2c) to the ground-based light profile of IC 1101 was limited, the downward departure of the inner light profile from the model reveals the partially depleted core. Porter et al. (1991) and Donzelli et al. (2011) claimed that IC 1101 does not have excess halo light, but see[8] Dressler (1979) and Uson et al. (1991). Donzelli et al. (2011) fit a single Sérsic model to the light profile of IC 1101, yielding an extremely large half-light radius $R_{\rm e} = 439$ kpc and $n \sim 5.8$, although they adopted a two-component Sérsic ($R^{1/n}$) plus exponential fit for their BCGs with $n \gtrsim 8$ and $R_{\rm e} \gtrsim 300$ kpc. The Donzelli et al. (2011) ground-based data with a seeing of FWHM = 1–2 arcsec did not have sufficient resolution to adequately resolve the core of IC 1101.

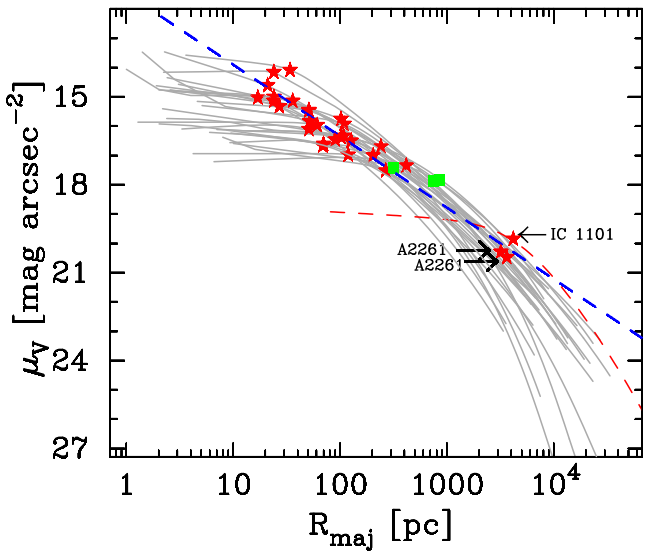

Figure 9. Compilation of core-Sérsic fits to the major-axis surface brightness profiles of all core galaxies from Dullo & Graham (2014, their table 2) together with the *V*-band core-Sérsic profile of IC 1101 from this work (red dashed curve). Red stars mark the break radius of the individual profiles. Green squares indicate the three galaxies (NGC 3842, Dullo & Graham 2014; NGC 1600, Thomas et al. 2016; NGC 4889, Dullo et al. in preparation) which have directly measured SMBH masses $M_{\rm BH} \gtrsim 10^{10}\,{\rm M}_\odot$ (McConnell et al. 2011; Thomas et al. 2016). For IC 1101, we show the major-axis core surface brightness ($\mu_{\rm b}$, Table 3), corrected for Galactic dust extinction, $(1+z)^4$ surface brightness dimming, and stellar evolution using the MILES stellar library (Vazdekis et al. 2010). For comparison, we include the hitherto largest core measured for A2261-BCG by Postman et al. (2012, $r_{\gamma=0.5} \sim 3.2$ kpc) and Bonfini & Graham (2016, $R_{\rm b} \sim 3.6$ kpc). IC 1101 and A2261-BCG follow the narrow sequence defined by the Dullo & Graham (2014) core-Sérsic galaxies (see Faber et al. 1997, their fig. 8). The (blue) dashed line is a least-squares fit taken from Dullo & Graham (2014, their table 3).

4.2 The large partially depleted core of IC 1101

Fig. 9 shows a compilation of major-axis core-Sérsic model profiles taken from Dullo & Graham (2014, their table 2) together with that for IC 1101. IC 1101 has one of the faintest *V*-band core (at $R_{\rm b}$ not to be confused with $R = 0$) surface brightnesses, $\mu_{\rm b} \sim 19.83$ mag arcsec^{-2}, corrected for Galactic dust extinction (~ -0.09 mag arcsec^{-2}), $(1+z)^4$ surface brightness dimming

[7] While Gonzalez et al. (2005) advocated an $R^{1/4}$ spheroid plus an $R^{1/4}$ outer stellar halo model to describe the profile of their BCGs, Gonzalez, Zabludoff & Zaritsky (2003) fit a two-component double-Sérsic model to the light profiles of BCGs.

[8] Dressler (1979) interpreted the luminosity, mass distribution and $\sigma(R)$ profile of IC 1101 using a three-component isotropic King model to account for the main body of the BCG, the stellar halo of accreted luminous galaxies and dark matter which was not included in the luminosity distribution model. The double nucleus that we modelled (Fig. 6) was not resolved in the Dressler (1979) image.

(~ -0.33 mag arcsec^{-2}) and stellar evolution from $z \sim 0.08$ to the present day, derived using the MILES stellar library[9] (Vazdekis et al. 2010), of $\sim +0.12$ mag arcsec^{-2}. For comparison, in addition to Fig. 9, see Lauer et al. (2007), Postman et al. (2012), Rusli et al. (2013) and Dullo & Graham (2014).

Although the break radius of IC 1101 ($R_b \sim 4.2 \pm 0.1$ kpc) is roughly an order of magnitude larger than those typically observed in core-Sérsic early-type galaxies, it closely follows the extrapolation of the R_b–μ_b sequence defined by other core-Sérsic galaxies (Dullo & Graham 2014, their table 3; Fig. 9). The next largest is ∼3.6 kpc in the A2261 BCG (Postman et al. 2012; Bonfini & Graham 2016) which is at redshift $z = 0.2248$, compared to $z = 0.0799$ for IC 1101. For comparison, the three core-Sérsic galaxies (NGC 1600, NGC 3842 and NGC 4889) housing very massive BHs ($M_{BH} \gtrsim 10^{10}$ M$_\odot$) have break radii $R_b \sim 300$–750 pc (Dullo & Graham 2014, $R_{b,NGC3842} \sim 315$ pc; Thomas et al. 2016, $R_{b,NGC1600} \sim 746$ pc; Dullo et al. in preparation, $R_{b,NGC4889} \sim 861$ pc).

Using the best-fitting parameters (Table 2), we find an absolute magnitude $M_{F702W} \approx -24.3$ mag for the spheroid of IC 1101. Correcting this for extinction, surface brightness dimming plus stellar evolution and using $V - F702W = 0.8$ (Fukugita, Shimasaku & Ichikawa 1995) yields $M_V \approx -23.8$ mag. This spheroid luminosity is very faint for the galaxy's large break radius, as the major-axis R_b–M_V relation for core-Sérsic galaxies (Dullo & Graham 2014, their table 3) predicts a small core ($R_{b,maj} \sim 400$ pc) for $M_V \approx -23.8$ mag, compared to IC 1101's $R_{b,maj} \sim 4.2$ kpc (Table 3). Given the 0.3 dex rms scatter (σ_s) for the R_b–M_V relation in the log (R_b) direction, the break radius of IC 1101 is 1.02 dex ($\sim 3.4\sigma_s$) above the R_b–M_V relation. Considering the spheroid + intermediate-scale component luminosity, the R_b–M_V relation (Dullo & Graham 2014) predicts $R_{b,maj} \sim 720$ pc, i.e. IC 1101's break radius is 0.77 dex ($\sim 2.6\,\sigma_s$) above the R_b–M_V relation.

4.3 Central stellar mass deficit (M_{def}) of IC 1101

In order to determine the stellar mass deficit of IC 1101, we follow the prescription in Dullo & Graham (2014, see also Graham 2004 and Ferrarese et al. 2006 who adopted a slightly different approach). We compute the difference in luminosity between the inwardly extrapolated outer Sérsic profile of the complete core-Sérsic model (equation 1) and the core-Sérsic model (equation 2). This yields a luminosity deficit log (L_{def}/L$_\odot$) $\sim 11.04^{+0.07}_{-0.07}$ in the $F702W$ band which corresponds to ≈ 27.7 per cent of the spheroid's luminosity prior to the core depletion. For comparison, L_{def} is ∼58 per cent of the luminosity of the intermediate-scale component. Moreover, Hopkins & Hernquist (2010) determined L_{def} using model-independent analysis of galaxy light profiles. They found values of L_{def} consistent with those of e.g. Graham (2004), Ferrarese et al. (2006) and Dullo & Graham (2014).

The depleted core has an $F450W - F702W$ colour of 1.81 ±0.03 (Fig. 8), which corresponds to a $V - I$ colour of 1.34 ±0.03 (Fukugita et al. 1995). Using the ($V - I$) colour–age–metallicity–M/L_V diagram (Graham & Spitler 2009) and assuming an old (12 Gyr) stellar population for the core yields $M/L_V \sim 5.2$. This implies $M/L_{F702W} \sim 4.5$ (Worthey 1994, his table 5A) and thus a stellar mass deficit (M_{def}) $\sim 4.9^{+1.03}_{-1.03} \times 10^{11}$ M$_\odot$ in IC 1101. The quoted 21 per cent uncertainty on M_{def} is based on the errors on the fit parameters (see Table 2).

[9] http://miles.iac.es/pages/stellar-libraries/miles-library.php

There is no evidence for the presence of dust lanes in the central regions of IC 1101 (see Figs 2, 3, 4 and 8) which could mimic a large apparent core/stellar mass deficit. Comparing fits to optical and near-IR light profiles, Ravindranath et al. (2001, their fig. 4) noted that nuclear dust lanes in galaxies typically tend to flatten the inner negative logarithmic slope (γ) of the profiles. For IC 1101, we find that increasing γ from 0.05 (Table 3) to 0.4 reduces the stellar mass deficit of IC 1101 only by ∼20 per cent.

Merritt (2006) simulated the evolution of SMBH binaries that are formed in galaxy merger remnants to quantify the relation between merger histories of core-Sérsic galaxies and their central stellar mass deficits. His simulations first revealed that the accumulated stellar mass deficit after $\mathcal{N}$ numbers of successive 'dry' major merges is $M_{def} \approx 0.5\mathcal{N}M_{BH}$, where M_{BH} is the final mass of the SMBH.

IC 1101 does not have a directly determined SMBH mass. Therefore, we estimate the SMBH mass using the M_{BH}–σ relation (Ferrarese & Merritt 2000; Gebhardt et al. 2000), the M_{BH}–L relation and M_{BH}–M_* relation (Dressler 1989; Kormendy & Richstone 1995; Magorrian et al. 1998). For $\sigma \sim 378$ km s^{-1} (HyperLeda), the Graham & Scott (2013) 'non-barred M_{BH}–σ relation predicts log M_{BH}/M$_\odot$ $\sim 9.68 \pm 0.47$. The McConnell & Ma (2013) M–σ relation for early-type galaxies including the two BCGs with very massive black holes (NGC 3842, M_{BH}/M$_\odot$ $\sim 9.7^{+3.0}_{-2.5} \times 10^9$ and NGC 4889, M_{BH}/M$_\odot$ $\sim 2.1^{+1.6}_{-1.6} \times 10^{10}$) and the Saglia et al. (2016, their table 11) M–σ relation for core-Sérsic elliptical galaxies predict log M_{BH}/M$_\odot$ $\sim 9.63 \pm 0.50$ and log M_{BH}/M$_\odot$ $\sim 9.82 \pm 0.49$, respectively. Using the V-band absolute magnitude of IC 1101's spheroid ($M_V \approx -23.8$ mag, i.e. $M_* \approx 1.5 \times 10^{12}$ M$_\odot$) and $B - V = 1.0$ (Fukugita et al. 1995), the Graham & Scott (2013) M_{BH}–L relation for core-Sérsic galaxies gives log M_{BH}/M$_\odot$ $\sim 9.99 \pm 0.40$ and the Savorgnan et al. (2016) M_{BH}–M_* relation and the Saglia et al. (2016, their table 11) M_{BH}–M_{Bu} relation for core-Sérsic ellipticals yield log M_{BH}/M$_\odot$ $\sim 10.11 \pm 0.47$ and log M_{BH}/M$_\odot$ $\sim 9.68 \pm 0.45$, respectively. Because M_{Bu} is the total, rather than the stellar, mass of the bulge (Saglia et al. 2016), the value of log M_{BH}/M$_\odot$ $\sim 9.68 \pm 0.45$ derived here using IC 1101's M_* and the M_{BH}–M_{Bu} relation is a lower limit.

It follows that $M_{def}/M_{BH} \approx 38$, 50 and 73–101 for SMBH masses determined using the M_{BH}–M_*, M_{BH}–L and M–σ relations, respectively. This translates to spheroid formation via an extremely frequent ($\mathcal{N} \gtrsim 76$) major mergers (Merritt 2006), if nothing else was occurring. Observations counting close galaxy pairs have led to estimates that today's massive galaxies may have experienced 0.5 to 6 major mergers since $z \sim 3$ (e.g. Bell et al. 2006; Conselice 2007; Bluck et al. 2012; Xu et al. 2012; Casteels et al. 2014), consistent with numbers estimated by theoretical models of galaxy mergers involving SMBHs (Haehnelt & Kauffmann 2002, their fig. 2). The M_{def}/M_{BH} ratio for IC 1101 is an order of magnitude higher than the typical M_{def}/M_{BH} values published in the literature (Graham 2004, $M_{def}/M_{BH} \sim 1$–2; Ferrarese et al. 2006, mean $M_{def}/M_{BH} \sim 2.4$; Hyde et al. 2008, mean $M_{def}/M_{BH} \sim 2.3$; Rusli et al. 2013, median $M_{def}/M_{BH} \sim 2.2$ and M_{def}/M_{BH} typically 0.2–10; Dullo & Graham 2013, 2014, $M_{def}/M_{BH} \sim 0.5$–4). In Section 4.4, we discuss that if the depleted core of IC 1101 was created by binary SMBHs with final merged mass $M_{BH} > 10^{10}$ M$_\odot$ and enhanced core scouring occurred due to a gravitational radiation-recoiled black hole (Gualandris & Merritt 2008), then the number of major mergers ($\mathcal{N}$) that the galaxy underwent would be $\lesssim 10$, in close agreement with observations and theories.

4.4 Formation of the A2029-BCG IC 1101

Massive galaxies are thought to build up hierarchically when smaller systems merge to form larger ones (Toomre 1977; White & Rees 1978). The high luminosities of BCGs, and their distinct physical properties and location near the centre of rich galaxy clusters suggest that they have experienced a higher number of mergers and accretion events than other luminous galaxies (e.g. Hausman & Ostriker 1978; De Lucia & Blaizot 2007; Rines, Finn & Vikhlinin 2007; von der Linden et al. 2007; Oliva-Altamirano et al. 2015). A2029, in which IC 1101 resides, is the second richest cluster in the Dressler (1978b, his table 3) sample of 13 very rich Abell (1958) clusters. Dressler (1978b, his fig. 1) showed that A2029 and A154 are the two clusters in his sample that have an excess number density (over $R \lesssim 4$ arcmin) with respect to the best King model fit to the cluster spatial distribution of galaxies. Dressler (1978a,b, 1979) also found a deficit of bright galaxies in the A2029 cluster, which led him to conclude that most of the massive galaxies in A2029 had been captured by and had merged with IC 1101, perhaps explaining the presence of the intermediate-scale and outer exponential halo components of IC 1101 (Fig. 6). Merritt (1985, see also Tremaine 1990), however, argued that such cannibalism is less efficient due to the clusters' high-velocity dispersion (but see Lauer 1988).

The findings by Dressler (1978a,b, 1979) may suggest that the extremely large core of IC 1101 is somewhat special and that the galaxy may have undergone a large number of dry major mergers involving binary SMBH scouring. None the less, $\mathcal{N} \gtrsim 76$ seems unrealistically large. In Section 4.3, we derived $\mathcal{N}$ assuming that (i) the extrapolations of the $M_{\rm BH}$–σ, $M_{\rm BH}$–L and $M_{\rm BH}$–M_* relations follow the sequence defined by the most massive BCGs and (ii) the cumulative scouring action of SMBH binaries is the sole mechanism that generated the large core in the galaxy. Not to be confused with galaxies whose $M_{\rm BH}/M_{\rm sph}$ ratio was overestimated because their disc light was overestimated, and thus their spheroid light was underestimated (see Savorgnan & Graham 2016); recent studies have revealed that the BHs in some BCGs are overmassive ($M_{\rm BH} \gtrsim 10^{10}\,{\rm M}_\odot$) compared to those predicted from $M_{\rm BH}$–σ and $M_{\rm BH}$–L relations (e.g. McConnell et al. 2011; Thomas et al. 2016). Also, the extrapolation of the relation between the black hole mass and the break radius ($M_{\rm BH}$–$R_{\rm b}$) for core-Sérsic galaxies (e.g. Dullo & Graham 2014, their equations 15, 16 and 17; Rusli et al. 2013, their equation 13; Thomas et al. 2016, their fig. 4) is such that IC 1101 would host an SMBH with $M_{\rm BH} \sim (4\text{–}10) \times 10^{10}\,{\rm M}_\odot$ (see also Laporte & White 2015) $\approx (1.7\text{–}3.2) \times \sigma_{\rm s}$ (rms scatter) larger than those estimated by the $M_{\rm BH}$–σ, $M_{\rm BH}$–L and $M_{\rm BH}$–M_* relations, thereby reducing the required merger rate for the galaxy to 10–20 major mergers, if the core depletion is only due to binary SMBHs. This possible existence of an overmassive black hole in IC 1101 supports the recent picture that the $M_{\rm BH}$–σ and $M_{\rm BH}$–L relations for elliptical galaxies and bulges may underestimate the SMBH masses of BCGs (e.g. McConnell et al. 2011; Hlavacek-Larrondo et al. 2012; Thomas et al. 2016).

Additional mechanisms, aside from binary SMBH scouring, may enhance a pre-existing depleted core and produce the large $M_{\rm def}/M_{\rm BH}$ ratio in IC 1101. For example, gravitationally 'recoiled' SMBHs, and the ensuing repeated oscillation about the centre of a 'dry' major merger remnant is invoked to explain $M_{\rm def}/M_{\rm BH} \sim 5$ rather than 0.5 (e.g. Redmount & Rees 1989; Boylan-Kolchin et al. 2004; Merritt et al. 2004; Gualandris & Merritt 2008). Therefore, if this process has occurred, then $\mathcal{N} \lesssim 10$ instead of 10–20 for IC 1101. In Fig. 3 (left), the residual structure reveals that the core of IC 1101 is slightly offset with respect to the outer isophotes, in agreement with the recoiled black hole oscillation scenario (see also Postman et al. 2012, their fig. 3).

We postulate that the intermediate-scale component and the outer halo of IC 1101 are in part consequences of galaxy merging and/or accretion of stars that were tidal stripped from less massive galaxies (e.g. Gallagher & Ostriker 1972). Furthermore, star formation in a cooling flow can add young stars to the halo of IC 1101. Clarke, Blanton & Sarazin (2004) found excess X-ray emission and high cooling flow rates in the A2029 cluster, concluding that the gas in the cluster has recently started cooling and forming stars (see also Walker et al. 2012; Paterno-Mahler et al. 2013). In addition, we find that the ejection of inner stars from the core of IC 1101 due to coalescing SMBHs and other mechanisms have created an extremely large stellar light deficit of $\log\,(L_{\rm def}/{\rm L}_\odot) \sim 11.04$, i.e. a V-band absolute magnitude of $M_{V,{\rm def}} \sim -22.8$ mag $\approx 1/3$ of the galaxy's spheroid luminosity prior to the scouring (Section 4.3). This high stellar light deficit for IC 1101 implies that ejected stars, which accumulate at large radii outside the core or escape from the galaxy at high velocities (Hills 1988), can impact the light profile outside the core region. This partly explains the presence of the intermediate-scale component with V-band absolute magnitude of $M_V \sim -23.4$ mag.

Overall, the large depleted core, ellipticity, orientation, the boxiness/disciness parameter (B_4), the relatively blue colour of the BCG at large radii (Figs 4, 6 and 8) and the velocity dispersion profile (Dressler 1979) favour the build-up of IC 1101 via a reasonably large number of dry major mergers ($\mathcal{N} \lesssim 10$) involving SMBHs (with the final merged SMBH mass $M_{\rm BH} \gtrsim 10^{10}\,{\rm M}_\odot$) and a number of accretion events. In this scenario, the central SMBH tidally disrupts any survived stellar nuclei of accreted/merged satellites, which otherwise would refill the depleted core (Faber et al. 1997; Boylan-Kolchin & Ma 2007; Bekki & Graham 2010). Our results suggest that the extremely large partially depleted core and $M_{\rm def}/M_{\rm BH}$ of IC 1101 maybe partly due to the actions of oscillatory core-passages by a gravitational wave-kicked SMBH.

5 CONCLUSIONS

We have provided a detailed discussion of a newly discovered and extremely large ($R_{\rm b} \sim 2.77$arcsec $\approx 4.2 \pm 0.1$ kpc) partially depleted core in the A2029 BCG IC 1101. Extracting the 1D surface brightness profile of IC 1101 from high-resolution *HST* WFPC2 imaging, we perform a careful four-component decomposition into a small elongated Gaussian nucleus, a core-Sérsic spheroid, a Sérsic intermediate-scale component and an exponential stellar halo. We also perform a 2D spheroid + intermediate-scale component + stellar halo + nucleus decomposition of IC 1101's *HST* WFPC2 image using IMFIT. The main findings from this work are as follows.

(1) The 1D spheroid + intermediate-scale component + stellar halo + nucleus model yields an excellent fit to the BCG's light profile. The rms residual scatter is below 0.02 mag arcsec^{-2}. We found good agreement between the 1D and 2D decompositions. In contrast, a 1D Gaussian nuclear component + Sérsic spheroid + Sérsic intermediate-scale component + exponential stellar halo model does not fit the light profile well, instead this fit creates a residual structure revealing the partially depleted core of the galaxy.

(2) IC 1101 has the largest core size (i.e. measured by the core-Sérsic break radius $R_{\rm b} \approx 4.2 \pm 0.1$ kpc) to date. This break radius is an order of magnitude larger than those typically measured for core-Sérsic galaxies (i.e. $R_{\rm b} \sim 20$–500 pc, e.g. Ferrarese et al. 2006;

Richings et al. 2011; Rusli et al. 2013; Dullo & Graham 2014). For comparison, Postman et al. (2012) modelled the semimajor axis profile of A2261-BCG and found the hitherto largest core ($r_{\gamma=0.5} \sim 3.2 \pm 0.1$ kpc), this large core was recently confirmed by Bonfini & Graham (2016) who measured $R_b \sim 3.6$ kpc.

(3) This depleted core in IC 1101 follows the extrapolation of the R_b–μ_b relation for core-Sérsic galaxies (e.g. Faber et al. 1997; Dullo & Graham 2014). However, the spheroid contains ∼25 per cent of the total galaxy light and has a *V*-band absolute magnitude (M_V) of −23.8 mag, which is faint for the large R_b. As such, the observed depleted core of IC 1101 is 1.02 dex $\approx 3.4\sigma_s$ (rms scatter) larger than that estimated from the R_b–M_V relation (Dullo & Graham 2014).

(4) We measured a stellar mass deficit at the centre of IC 1101 $\approx M_{def} \sim 4.9 \times 10^{11}$ M$_\odot$, (a luminosity deficit L_{def}/L$_\odot \sim 1.1 \times 10^{11}$ in the *F*702*W* band ≈ 28 per cent of the spheroid luminosity before the core depletion). Estimating the black hole mass of the galaxy using the spheroid's stellar mass ($M_* \sim 1.1 \times 10^{12}$ M$_\odot$), luminosity ($M_V \sim -23.8$ mag) and velocity dispersion ($\sigma \sim 378$ km s^{-1}) yields M_{def}/M_{BH} ratios of ∼ 38, 50 and 73–101, respectively. This figure translates to spheroid formation via an unrealistically large ($\mathcal{N} \gtrsim 76$) number of 'dry' major mergers. However, the extrapolation of the relation between the black hole mass and the break radius (M_{BH}–R_b) for core-Sérsic galaxies (Rusli et al. 2013; Dullo & Graham 2014; Thomas et al. 2016) suggests IC 1101 hosts an overmassive BH ($M_{BH} \sim (4\text{–}10) \times 10^{10}$ M$_\odot$) ≈ (1.7–3.2) × σ_s (rms scatter) larger than those SMBH masses estimated by the M_{BH}–σ and M_{BH}–*L* relations, thereby reducing the merger rate for the galaxy to $\mathcal{N} \lesssim 10$, in close agreement with observational and theoretical merger rates of massive galaxies. An additional mechanism that can contribute to the large core/mass deficit is oscillatory core passages by a recoiled SMBH. It is important to investigate the reasons why BCGs with extremely large depleted cores and stellar mass deficits similar to IC 1101 are quite rare, especially within a distance of ∼100 Mpc.

ACKNOWLEDGEMENTS

BTD thanks the referee for their careful reading of the paper and useful suggestions. BTD acknowledges support from a Spanish postdoctoral fellowship 'Ayudas para la atracción del talento investigador. Modalidad 2: jóvenes investigadores, financiadas por la Comunidad de Madrid' under grant number 2016-T2/TIC-2039. BTD and JHK acknowledge financial support from the Spanish Ministry of Economy and Competitiveness (MINECO) under grant number AYA2013-41243-P. JHK acknowledges financial support from the European Union's Horizon 2020 research and innovation programme under Marie Skłodowska-Curie grant agreement No. 721463 to the SUNDIAL ITN network, and from the Spanish Ministry of Economy and Competitiveness (MINECO) under grant number AYA2016-76219-P. AWG was supported under the Australian Research Council's funding scheme (DP17012923). JHK thanks the Astrophysics Research Institute of Liverpool John Moores University for their hospitality, and the Spanish Ministry of Education, Culture and Sports for financial support of his visit there, through grant number PR2015-00512. This research used APLPY, an open-source plotting package for PYTHON (Robitaille & Bressert 2012).

REFERENCES

Abell G. O., 1958, ApJS, 3, 211
Antonini F., Merritt D., 2012, ApJ, 745, 83
Arca-Sedda M., Capuzzo-Dolcetta R., Antonini F., Seth A., 2015, ApJ, 806, 220
Arca-Sedda M., Capuzzo-Dolcetta R., Spera M., 2016, MNRAS, 456, 2457
Begelman M. C., Blandford R. D., Rees M. J., 1980, Nature, 287, 307
Bekenstein J. D., 1973, ApJ, 183, 657
Bekki K., Graham A. W., 2010, ApJ, 714, L313
Bell E. F. et al., 2006, ApJ, 640, 241
Bender R., Kormendy J., Cornell M. E., Fisher D. B., 2015, ApJ, 807, 56
Bertin E., Arnouts S., 1996, A&AS, 117, 393
Binney J., Mamon G. A., 1982, MNRAS, 200, 361
Blanton M. R., Kazin E., Muna D., Weaver B. A., Price-Whelan A., 2011, AJ, 142, 31
Bluck A. F. L., Conselice C. J., Buitrago F., Grützbauch R., Hoyos C., Mortlock A., Bauer A. E., 2012, ApJ, 747, 34
Bonfini P., 2014, PASP, 126, 935
Bonfini P., Graham A. W., 2016, ApJ, 829, 81
Bonfini P., Dullo B. T., Graham A. W., 2015, ApJ, 807, 136
Boylan-Kolchin M., Ma C.-P., 2007, MNRAS, 374, 1227
Boylan-Kolchin M., Ma C.-P., Quataert E., 2004, ApJ, 613, L37
Buote D. A., Tsai J. C., 1996, ApJ, 458, 27
Byun Y.-I. et al., 1996, AJ, 111, 1889
Carollo C. M., Franx M., Illingworth G. D., Forbes D. A., 1997, ApJ, 481, 710
Carter D., 1977, MNRAS, 178, 137
Carter D., Inglis I., Ellis R. S., Efstathiou G., Godwin J. G., 1985, MNRAS, 212, 471
Carter D., Bridges T. J., Hau G. K. T., 1999, MNRAS, 307, 131
Casteels K. R. V. et al., 2014, MNRAS, 445, 1157
Ciambur B. C., 2016, PASA, 33, e062
Clarke T. E., Blanton E. L., Sarazin C. L., 2004, ApJ, 616, 178
Condon J. J., Cotton W. D., Greisen E. W., Yin Q. F., Perley R. A., Taylor G. B., Broderick J. J., 1998, AJ, 115, 1693
Conselice C. J., 2007, in Combes F., Palous J., eds, Proc. IAU Symp. 235, Galaxy Evolution Across the Hubble Time. Cambridge Univ. Press, Cambridge, p. 381
Crane P. et al., 1993, AJ, 106, 1371
De Lucia G., Blaizot J., 2007, MNRAS, 375, 2
de Vaucouleurs G., 1948, Ann. Astrophys., 11, 247
de Vaucouleurs G., de Vaucouleurs A., Corwin H. G. Jr, Buta R. J., Paturel G., Fouqué P., 1991, Third Reference Catalogue of Bright Galaxies, Vol. I. Springer, New York
Debattista V. P., Ferreras I., Pasquali A., Seth A., De Rijcke S., Morelli L., 2006, ApJ, 651, L97
Donzelli C. J., Muriel H., Madrid J. P., 2011, ApJS, 195, 15
Dressler A., 1978a, ApJ, 223, 765
Dressler A., 1978b, ApJ, 226, 55
Dressler A., 1979, ApJ, 231, 659
Dressler A., 1981, ApJ, 243, 26
Dressler A., 1989, in Osterbrock D. E., Miller J. S., eds, Proc. IAU Symp. 134, Active Galactic Nuclei. Kluwer, Dordrecht, p. 217
Dullo B. T., Graham A. W., 2012, ApJ, 755, 163
Dullo B. T., Graham A. W., 2013, ApJ, 768, 36
Dullo B. T., Graham A. W., 2014, MNRAS, 444, 2700
Dullo B. T., Graham A. W., 2015, ApJ, 798, 55
Dullo B. T., Martínez-Lombilla C., Knapen J. H., 2016, MNRAS, 462, 3800
Ebisuzaki T., Makino J., Okumura S. K., 1991, Nature, 354, 212
Erwin P., 2015, ApJ, 799, 226
Faber S. M. et al., 1997, AJ, 114, 1771
Ferrarese L., Merritt D., 2000, ApJ, 539, L9
Ferrarese L., van den Bosch F. C., Ford H. C., Jaffe W., O'Connell R. W., 1994, AJ, 108, 1598
Ferrarese L. et al., 2006, ApJS, 164, 334
Fisher D., Illingworth G., Franx M., 1995, ApJ, 438, 539
Fitchett M. J., 1983, MNRAS, 203, 1049
Forbes D. A., Franx M., Illingworth G. D., 1995, AJ, 109, 1988
Fukugita M., Shimasaku K., Ichikawa T., 1995, PASP, 107, 945
Gallagher J. S., III, Ostriker J. P., 1972, AJ, 77, 288
Gebhardt K. et al., 1996, AJ, 112, 105

Gebhardt K. et al., 2000, ApJ, 539, L13
Gebhardt K. et al., 2003, ApJ, 583, 92
Goerdt T., Moore B., Read J. I., Stadel J., 2010, ApJ, 725, 1707
Gonzalez A. H., Zabludoff A. I., Zaritsky D., 2003, Ap&SS, 285, 67
Gonzalez A. H., Zabludoff A. I., Zaritsky D., 2005, ApJ, 618, 195
Graham A. W., 2004, ApJ, 613, L33
Graham A. W., Driver S. P., 2005, PASA, 22, 118
Graham A. W., Scott N., 2013, ApJ, 764, 151
Graham A. W., Spitler L. R., 2009, MNRAS, 397, 2148
Graham A. W., Erwin P., Trujillo I., Asensio Ramos A., 2003, AJ, 125, 2951
Grillmair C. J., Faber S. M., Lauer T. R., Baum W. A., Lynds R. C., O'Neil E. J., Jr, Shaya E. J., 1994, AJ, 108, 102
Gualandris A., Merritt D., 2008, ApJ, 678, 780
Haehnelt M. G., Kauffmann G., 2002, MNRAS, 336, L61
Hausman M. A., Ostriker J. P., 1978, ApJ, 224, 320
Hills J. G., 1988, Natur, 331, 687
Hlavacek-Larrondo J., Fabian A. C., Edge A. C., Hogan M. T., 2012, MNRAS, 424, 224
Hopkins P. F., Hernquist L., 2010, MNRAS, 407, 447
Hyde J. B., Bernardi M., Sheth R. K., Nichol R. C., 2008, MNRAS, 391, 1559
Jaffe W., Ford H. C., O'Connell R. W., van den Bosch F. C., Ferrarese L., 1994, AJ, 108, 1567
Jedrzejewski R. I., 1987, MNRAS, 226, 747
Kelson D. D., Zabludoff A. I., Williams K. A., Trager S. C., Mulchaey J. S., Bolte M., 2002, ApJ, 576, 720
Khosroshahi H. G., Ponman T. J., Jones L. R., 2006, MNRAS, 372, L68
King I. R., 1978, ApJ, 222, 1
King I. R., Minkowski R., 1966, ApJ, 143, 1002
Kormendy J., Bender R., 2009, ApJ, 691, L142
Kormendy J., Ho L. C., 2013, ARA&A, 51, 511
Kormendy J., Richstone D., 1995, ARA&A, 33, 581
Kormendy J., Dressler A., Byun Y. I., Faber S. M., Grillmair C., Lauer T. R., Richstone D., Tremaine S., 1994, in Meylan G., Prugniel P., eds, ESO Conf. Ser. Vol. 49, Dwarf Galaxies. ESO, Garching, p. 147
Krist J., 1995, in Shaw R. A., Payne H. E., Hayes J. J. E., Proc. ASP Conf. Ser. Vol. 77, Astronomical Data Analysis Software and Systems IV. Astron. Soc. Pac., San Francisco, p. 349
Kulkarni G., Loeb A., 2012, MNRAS, 422, 1306
Laine S., van der Marel R. P., Lauer T. R., Postman M., O'Dea C. P., Owen F. N., 2003, AJ, 125, 478
Laporte C. F. P., White S. D. M., 2015, MNRAS, 451, 1177
Lauer T. R., 1985, ApJ, 292, 104
Lauer T. R., 1988, ApJ, 325, 49
Lauer T. R. et al., 1995, AJ, 110, 2622
Lauer T. R. et al., 1996, ApJ, 471, L79
Lauer T. R. et al., 2005, AJ, 129, 2138
Lauer T. R. et al., 2007, ApJ, 662, 808
López-Cruz O., Añorve C., Birkinshaw M., Worrall D. M., Ibarra-Medel H. J., Barkhouse W. A., Torres-Papaqui J. P., Motta V., 2014, ApJ, 795, L31
Lugger P. M., 1984, ApJ, 286, 106
McConnell N. J., Ma C.-P., 2013, ApJ, 764, 184
McConnell N. J., Ma C.-P., Gebhardt K., Wright S. A., Murphy J. D., Lauer T. R., Graham J. R., Richstone D. O., 2011, Natur, 480, 215
Madrid J. P., Donzelli C. J., 2016, ApJ, 819, 50
Magorrian J. et al., 1998, AJ, 115, 2285
Matthews T. A., Morgan W. W., Schmidt M., 1964, ApJ, 140, 35
Mazzalay X., Thomas J., Saglia R. P., Wegner G. A., Bender R., Erwin P., Fabricius M. H., Rusli S. P., 2016, MNRAS, 462, 2847
Merritt D., 1985, ApJ, 289, 18
Merritt D., 2006, ApJ, 648, 976
Merritt D., Milosavljević M., Favata M., Hughes S. A., Holz D. E., 2004, ApJ, 607, L9
Milosavljević M., Merritt D., 2001, ApJ, 563, 34
Oemler A., Jr, 1976, ApJ, 209, 693
Oliva-Altamirano P. et al., 2015, MNRAS, 449, 3347
Paterno-Mahler R., Blanton E. L., Randall S. W., Clarke T. E., 2013, ApJ, 773, 114
Paturel G., Petit C., Prugniel P., Theureau G., Rousseau J., Brouty M., Dubois P., Cambrésy L., 2003, A&A, 412, 45
Pierini D., Zibetti S., Braglia F., Böhringer H., Finoguenov A., Lynam P. D., Zhang Y.-Y., 2008, A&A, 483, 727
Porter A. C., Schneider D. P., Hoessel J. G., 1991, AJ, 101, 1561
Postman M., Lauer T. R., 1995, ApJ, 440, 28
Postman M. et al., 2012, ApJ, 756, 159
Quinlan G. D., Hernquist L., 1997, New Astron., 2, 533
Ravindranath S., Ho L. C., Peng C. Y., Filippenko A. V., Sargent W. L. W., 2001, AJ, 122, 653
Redmount I. H., Rees M. J., 1989, Comments Astrophys., 14, 165
Rest A., van den Bosch F. C., Jaffe W., Tran H., Tsvetanov Z., Ford H. C., Davies J., Schafer J., 2001, AJ, 121, 2431
Richings A. J., Uttley P., Körding E., 2011, MNRAS, 415, 2158
Rines K., Finn R., Vikhlinin A., 2007, ApJ, 665, L9
Robitaille T., Bressert E., 2012, Astrophysics Source Code Library, record (ascl:1208.017)
Rusli S. P., Erwin P., Saglia R. P., Thomas J., Fabricius M., Bender R., Nowak N., 2013, AJ, 146, 160
Saglia R. P. et al., 2016, ApJ, 818, 47
Savorgnan G. A. D., Graham A. W., 2016, MNRAS, 457, 320
Savorgnan G. A. D., Graham A. W., Marconi A., Sani E., 2016, ApJ, 817, 21
Schombert J. M., 1986, ApJS, 60, 603
Schombert J. M., 1987, ApJS, 64, 643
Seigar M. S., Graham A. W., Jerjen H., 2007, MNRAS, 378, 1575
Sembach K. R., Tonry J. L., 1996, AJ, 112, 797
Sérsic J. L., 1963, Bol. Asociacion Argentina Astron., 6, 41
Sérsic J. L., 1968, Atlas de Galaxias Australes. Observatorio Astronomico, Universidad Nacional de Córdoba, Córdoba
Stewart G. C., Fabian A. C., Jones C., Forman W., 1984, ApJ, 285, 1
Thomas J., Saglia R. P., Bender R., Erwin P., Fabricius M., 2014, ApJ, 782, 39
Thomas J., Ma C.-P., McConnell N. J., Greene J. E., Blakeslee J. P., Janish R., 2016, Nature, 532, 340
Tonry J. L., 1987, in de Zeeuw P. T., ed., Proc. IAU Symp. 127, Structure and Dynamics of Elliptical Galaxies. Reidel, Dordrecht, p. 89
Toomre A., 1977, in Tinsley B. M., Larson R. B., eds, The Evolution of Galaxies and Stellar Populations. Yale Univ. Press, New Haven, CT, p. 401
Tremaine S., 1990, in Wielen R., ed., Dynamics and Interactions of Galaxies. Springer-Verlag, Berlin, p. 394
Trujillo I., Aguerri J. A. L., Cepa J., Gutiérrez C. M., 2001a, MNRAS, 321, 269
Trujillo I., Aguerri J. A. L., Cepa J., Gutiérrez C. M., 2001b, MNRAS, 328, 977
Trujillo I., Erwin P., Asensio Ramos A., Graham A. W., 2004, AJ, 127, 1917
Uson J. M., Boughn S. P., Kuhn J. R., 1991, ApJ, 369, 46
van den Bosch F. C., Ferrarese L., Jaffe W., Ford H. C., O'Connell R. W., 1994, AJ, 108, 1579
Vazdekis A., Sánchez-Blázquez P., Falcón-Barroso J., Cenarro A. J., Beasley M. A., Cardiel N., Gorgas J., Peletier R. F., 2010, MNRAS, 404, 1639
von der Linden A., Best P. N., Kauffmann G., White S. D. M., 2007, MNRAS, 379, 867
Walker S. A., Fabian A. C., Sanders J. S., George M. R., Tawara Y., 2012, MNRAS, 422, 3503
White S. D. M., Rees M. J., 1978, MNRAS, 183, 341
Worthey G., 1994, ApJS, 95, 107
Xu C. K., Zhao Y., Scoville N., Capak P., Drory N., Gao Y., 2012, ApJ, 747, 85
Zibetti S., White S. D. M., Schneider D. P., Brinkmann J., 2005, MNRAS, 358, 949

This paper has been typeset from a TEX/LATEX file prepared by the author.